CHEMISTRY OF MATERIALS
Article

Chem. Mater. **2010,** *22,* 5165–5173 5165
DOI:10.1021/cm101019p

Twisted Nanotubes Formed from Ultrashort Amphiphilic Peptide I_3K and Their Templating for the Fabrication of Silica Nanotubes

Hai Xu,*,† Yuming Wang,† Xin Ge,† Shuyi Han,† Shengjie Wang,† Peng Zhou,† Honghong Shan,† Xiubo Zhao,‡ and Jian R. Lu*,‡

†*State Key Laboratory of Heavy Oil Processing and Centre for Bioengineering and Biotechnology, China University of Petroleum (East China), 66 Changjiang West Road, Qingdao 266555, China, and* ‡*Biological Physics Laboratory, School of Physics and Astronomy, University of Manchester, Schuster Building, Manchester M13 9PL, U.K.*

Received April 13, 2010. Revised Manuscript Received July 26, 2010

Many de novo designed amphiphilic peptides capable of self-assembly and further structural templating into hierarchical organizations such as nanofibers and gels carry more than 10 amino acid residues. A curious question is now raised about the minimal size that is required for initiating amphiphilically driven nanostructuring. In this work, we show that ultrashort peptides I_3K and L_3K could readily self-assemble into stable nanostructures. While L_3K formed spherical nanospheres with diameters of ~10−15 nm, I_3K self-assembled into nanotubes with diameters of ~10 nm and lengths of $> 5\ \mu$m. I_3K nanotubes were very smooth and carried defined pitches of twisting. The difference could arise from the different β-sheet promoting power between isoleucine and leucine, suggesting that while hydrophobic interaction was dominant in the formation of L_3K nanospheres hydrogen bonding governed the templating of antiparallel β-sheets and the subsequent formation of I_3K nanotubes. Because of their extreme stability against heating or exposure to organic solvents, I_3K nanotubes were used as templates for silicification from the hydrolysis of organosilicate precursors using TEOS (tetraethoxysilane). The lysine groups on the inner and outer nanotube surfaces worked to catalyze silicification, leading to the formation of silica nanotubes, which is evident from both AFM and TEM imaging. The formation of interesting nanotubes and nanospheres as demonstrated from very short peptide amphiphiles is significant for further exploration of their use in technological applications.

Introduction

Molecular self-assembly is ubiquitous in biological systems through which a wide variety of architectures and molecular machines are built from constituent species.[1] Study of molecular self-assembly offers useful insights into sophisticated biological processes as well as inspirations for developing novel technological applications. Tremendous interest in peptide self-assembly has recently arisen because of the huge potential of the assembled nanostructures in an array of biomedical and technological applications.[2−12] Because of the great diversity in the composition and properties of constituent amino acids, potential self-assembling peptides could be numerous. The stable and well-ordered structural

*To whom correspondence should be addressed. H.X.: telephone, (+86)532-8698-1569; e-mail, xuh@upc.edu.cn. J.R.L.: telephone, (+44)-161-200-3926; e-mail, j.lu@manchester.ac.uk.

(1) (a) Lehn, J.-M. *Science* **2002**, *295*, 2400. (b) Whitesides, G. M.; Grzybowski, B. *Science* **2002**, *295*, 2418. (c) Whitesides, G. M.; Boncheva, M. *Proc. Natl. Acad. Sci. U.S.A.* **2002**, *99*, 4769.

(2) (a) Ghadiri, M. R.; Granja, J. R.; Milligan, R. A.; Mcree, D. E.; Khazanovich, N. *Nature* **1993**, *366*, 324. (b) Ghadiri, M. R.; Granja, J. R.; Buehler, L. K. *Nature* **1994**, *369*, 301. (c) Fernandez-Lopez, S.; Kim, H.-S.; Choi, E. C.; Delgado, M.; Granja, J. R.; Khasanov, A.; Kraehenbuehl, K.; Long, G.; Weinberger, D. A.; Wilcoxen, K. M.; Ghadiri, M. R. *Nature* **2001**, *412*, 452.

(3) (a) Zhang, S.; Holmes, T. C.; Dipersio, C. M.; Hynes, R. O.; Su, X.; Rich, A. *Biomaterials* **1995**, *16*, 1385. (b) Holmes, T.; Delacalle, S.; Su, X.; Rich, A.; Zhang, S. *Proc. Natl. Acad. Sci. U.S.A.* **2000**, *97*, 6728. (c) Ellis-Behnke, R. G.; Liang, Y.-X.; You, S.-W.; Tay, D. K. C.; Zhang, S.; So, K.-F.; Schneider, G. E. *Proc. Natl. Acad. Sci. U.S.A.* **2006**, *103*, 5054.

(4) (a) Aggeli, A.; Bell, M.; Boden, N.; Keen, J. N.; Knowles, P. F.; Mcleish, T. C.; Pitkeathly, M.; Radford, S. E. *Nature* **1997**, *386*, 259. (b) Meegan, J. E.; Aggeli, A.; Boden, N.; Brydson, R.; Brown, A. P.; Carrick, L.; Brough, A. R.; Hussain, A.; Ansell, R. J. *Adv. Funct. Mater.* **2004**, *14*, 31. (c) Whitehouse, C.; Fang, J.; Aggeli, A.; Bell, M.; Brydson, R.; Fishwick, C. W. G.; Henderson, J. R.; Knobler, C. M.; Owens, R. W.; Thomson, N. H.; Smith, D. A.; Boden, N. *Angew. Chem., Int. Ed.* **2005**, *44*, 1965.

(5) (a) Hartgerink, J. D.; Beniash, E.; Stupp, S. I. *Science* **2001**, *294*, 1684. (b) Cui, H.; Muraoka, T.; Cheetham, A. G.; Stupp, S. I. *Nano Lett.* **2009**, *9*, 945. (c) Silva, G. A.; Czeisler, C.; Niece, K. L.; Beniash, E.; Harrington, D. A.; Kessler, J. A.; Stupp, S. I. *Science* **2004**, *303*, 1352. (d) Sone, E. D.; Stupp, S. I. *J. Am. Chem. Soc.* **2004**, *126*, 12756. (e) Li, L.-S.; Stupp, S. I. *Angew. Chem., Int. Ed.* **2005**, *44*, 1833.

(6) (a) Reches, M.; Gazit, E. *Science* **2003**, *300*, 625. (b) Gazit, E. *FEBS J.* **2007**, *274*, 317. (c) Reches, M.; Gazit, E. *Nat. Nanotechnol.* **2006**, *1*, 195.

(7) (a) Zhang, S. *Nat. Biotechnol.* **2003**, *21*, 1171. (b) Zhang, S.; Marini, D. M.; Hwang, W.; Santoso, S. *Curr. Opin. Chem. Biol.* **2002**, *6*, 865.

(8) (a) Gao, X.; Matsui, H. *Adv. Mater.* **2005**, *17*, 2037. (b) Banerjee, I. A.; Yu, L.; Matsui, H. *Proc. Natl. Acad. Sci. U.S.A.* **2003**, *100*, 14678. (c) Matsui, H.; Gologan, B. *J. Phys. Chem. B* **2000**, *104*, 3383. (d) Matsui, H.; Douberly, G. E. *Langmuir* **2001**, *17*, 7918. (e) Matsui, H.; MacCuspie, R. *Nano Lett.* **2001**, *1*, 671.

(9) (a) Ulijn, R. V.; Smith, A. M. *Chem. Soc. Rev.* **2008**, *37*, 664. (b) Smith, A. M.; Williams, R. J.; Tang, C.; Coppo, P.; Collins, R. F.; Turner, M. L.; Saiani, A.; Ulijn, R. V. *Adv. Mater.* **2008**, *20*, 37.

Published on Web 08/17/2010

morphologies of the peptide assemblies are largely achieved through the exquisite combination of noncovalent interactions that are weak but strong when the number is large, including ionic interactions, hydrophobic interactions, hydrogen bonding, and $\pi-\pi$ stacking. Although the specific and quantitative roles of these interactions still need to be quantified, development of basic rationales to link primary sequences to three-dimensional structures will represent a major step toward the de novo design of peptide sequences targeting specific applications.

Practical applications will always favor short self-assembling peptides because they are easier to produce in large scale and their structure−function relations can be more easily established. Following our previous work to demonstrate the surface and interfacial assembly of 14-mer and 15-mer peptide sequences, we have recently shown shorter peptides containing 5−10 amino acid residues could also self-assemble into stable nanostructures at the interface and in solution.[12] In this work, we show that even shorter amphiphilic peptides such as I_3K (Ac-IIIK-NH_2) and L_3K (Ac-LLLK-NH_2) can self-assemble into stable and well-defined nanostructures. More interestingly, we show that minor differences in the structure of L and I have hugely different influences on nanostructuring: while L_3K formed nanospheres in aqueous solution at neutral pH, I_3K promoted the formation of long nanotubes. Isoleucine is a β-branched hydrophobic amino acid that has a strong propensity to adopt β-sheet conformation.[13] Secondary structure studies revealed the lack of any significant β-sheet in the self-assembled L_3K, but the β-sheet conformation was dominant in the I_3K nanostructured solution. These studies thus revealed that while hydrophobic interaction was dominant in forming the L_3K nanospheres, hydrogen bonding must be dominant in forming I_3K nanotubes. The hallmark from these I_3K nanotubes is that their lengths are well over 5 μm while their diameters were only ~10 nm. Furthermore, the assembled I_3K nanostructures were stable and displayed structural and morphological integrity against rather extreme conditions. Moreover, we have successfully applied the self-assembled nanostructures as templates for controlling silica deposition under benign conditions. Smooth silica nanotubes have been manufactured from the hierarchical bottom-up approach using I_3K nanotubes as templates.

Experimental Section

Peptides were synthesized using the standard Fmoc solid-phase synthesis strategy from natural L-amino acids on a CEM Liberty microwave peptide synthesizer. The synthesis was initiated on a Rink-amide resin. After Fmoc deprotection, the N-terminus was capped with acetic anhydride and the C-terminus was amidated, thereby generating one positive charge per molecule (from the lysine residue side chain) at neutral pH. After cleavage from the resin with an aqueous mixture of 94% trifluoroacetic acid, peptides were precipitated with cold ethyl ether at least six times to reach a high purity of >98%, as evident from HPLC and MALDI-TOF MS analysis (see Figures S1 and S2 of the Supporting Information). Because of the short sequence, these simple surfactant-like peptides were extremely easy to synthesize with high yield and purity. This advantage is rather appealing for their large scale production and technological applications based on self-assembly into well-defined nanostructures. Further information about peptide synthesis, purification, and characterization is given in the Supporting Information.

In spite of the strong hydrophobicity of isoleucine, I_3K exhibited high solubility in aqueous solution because of its short sequence and inherent amphiphilic nature. The peptide was dissolved in pure water (Milli-Q) with the solution pH around 6. The stock solution was created at 10 mM, with the solution pH adjusted to 5, 7, and 9 for SANS and other studies by using a minute amount of dilute HCl and NaOH solution.

Solutions aged for more than 3 days were used for transmission electron microscopy (TEM) to characterize the nanostructures at concentrations of 4 and 10 mM. The peptide samples were negatively stained with 2% (w/v) uranyl acetate in water and subsequently viewed with a JEOL JEM-2100UHR electron microscope operated at 200 kV. The atomic force microscope (AFM) measurements were performed on a commercial Nanoscope IVa MultiMode AFM (Digital Instruments, Santa Barbara, CA) in tapping mode, using a TESP silicon probe (Veeco, Santa Barbara, CA) having a nominal spring constant of 42 N/m and a typical frequency of 300 kHz. AFM phase imaging was effective at revealing the helical structural features (Figure 3b), and topographic imaging was useful at showing height variations (Figure 3a,c), both types of images being obtained concurrently from the same surface area.

Measurements of fluorescence spectra were performed on a Horiba Jobin Yvon Fluoromax-4 spectrometer at 25 °C. Pyrene was used as the probe, and its concentration in the peptide solution was fixed at 10^{-5} mM. The probe was excited at a wavelength of 335 nm, and the emission spectra were recorded over the scanning range of 350−550 nm. The rheological properties of the peptide solution were assessed with a Thermo Haake MARS rheometer at 25 °C, by using a cone plate geometry. The cone diameter is 35 mm, and the gap between the cone and the base plate is 0.105 mm. Dynamic properties of G' and G'' were measured using frequency sweeping performed at a constant stress of 0.1 Pa (chosen in the linear viscoelastic range from 0.01 to 1.0 Pa) over a frequency range of 0.1−10 Hz.

The circular dichroism (CD) measurements were taken on a Bio-Logic MOS 450 instrument, using a 1 mm quartz cell at wavelengths ranging from 190 to 250 nm. The CD spectra were

(10) (a) Ryu, J.; Park, C. B. *Angew. Chem., Int. Ed.* **2009**, *48*, 4820. (b) Yan, X.; He, Q.; Wang, K.; Duan, L.; Cui, Y.; Li, J. *Angew. Chem., Int. Ed.* **2007**, *46*, 2431. (c) Yan, X.; Cui, Y.; He, Q.; Wang, K.; Li, J.; Mu, W.; Wang, B.; Ou-Yang, Z.-C. *Chem.—Eur. J.* **2008**, *14*, 5974.

(11) (a) Vauthey, S.; Santoso, S.; Gong, H.; Watson, N.; Zhang, S. *Proc. Natl. Acad. Sci. U.S.A.* **2002**, *99*, 5355. (b) von Maltzahn, G.; Vauthey, S.; Santoso, S.; Zhang, S. *Langmuir* **2003**, *19*, 4332. (c) Yeh, J. I.; Du, S.; Tortajada, A.; Paulo, J.; Zhang, S. *Biochemistry* **2005**, *44*, 16912. (d) Kiley, P.; Zhao, X.; Vaughn, M.; Baldo, M. A.; Bruce, B. D.; Zhang, S. *PLoS Biol.* **2005**, *3*, 1180. (e) Zhao, X.; Nagai, Y.; Reeves, P. J.; Kiley, P.; Khorana, H. G.; Zhang, S. *Proc. Natl. Acad. Sci. U.S.A.* **2006**, *103*, 17707.

(12) (a) Wang, J.; Han, S.; Meng, G.; Xu, H.; Xia, D.; Zhao, X.; Schweins, R.; Lu, J. R. *Soft Matter* **2009**, *5*, 3870. (b) Zhao, X.; Pan, F.; Perumal, S.; Xu, H.; Lu, J. R.; Webster, J. R. P. *Soft Matter* **2009**, *5*, 1630. (c) Xu, H.; Wang, J.; Han, S.; Wang, J.; Yu, D.; Zhang, H.; Xia, D.; Zhao, X.; Waigh, T. A.; Lu, J. R. *Langmuir* **2009**, *25*, 4115. (d) Lu, J. R.; Perumal, S.; Hopkinson, I.; Webster, J. R. P.; Penfold, J.; Hwang, W.; Zhang, S. *J. Am. Chem. Soc.* **2004**, *126*, 8940. (e) Lu, J. R.; Perumal, S.; Powers, E. T.; Kelly, J. W.; Webster, J. R. P.; Penfold, J. *J. Am. Chem. Soc.* **2003**, *125*, 3751.

(13) Arfmann, H. A.; Labitzke, R.; Wagner, K. G. *Biopolymers* **1977**, *16*, 1815.

recorded at 22−23 °C with a 0.5 nm bandwidth and a scan speed of 50 nm/min. Each spectrum was corrected by a baseline measured with the same solvent in the same cell. The intensity of the CD spectra is expressed as $[\theta] \times 10^{-3}$ degrees square centimeters per decimole. Infrared spectra of the peptide solution were recorded on a Nicolet 6700 FTIR spectrometer at 22−23 °C. An ARK HATR accessory (Thermo Electron) equipped with a ZnSe crystal and a trough sampling plate was used in the IR measurements.

SANS measurements were taken on the white beam time-of-flight scattering instrument, LOQ, at ISIS Facility [Rutherford Appleton Laboratory (RAL), Didcot, Oxford, U.K.]. The wavelength range used was from 2 to 10 Å, and the typical wave vector (Q) range measured was from 0.006 to 0.29 $Å^{-1}$. All samples were placed in 2 mm path fused silica cells. Data were corrected for the wavelength dependence of the incident spectrum, the measured sample transmission, and relative detector efficiencies, prior to the subtraction of background from respective D_2O buffers. Absolute scaling was achieved by comparison to the scattering from a partially deuterated polystyrene standard. For each peptide, the first SANS measurement was taken at pH 5, and the subsequent pH increase was achieved via addition of a minimal amount of dilute HCl or NaOH in D_2O. Solutions with lower concentrations of peptide were diluted from the 10 mM stock solution. All the SANS runs were conducted at 25 °C. Data modeling was conducted using the FISH2 fitting program developed by R. K. Heenan at RAL. It proceeded by testing simple geometrical shapes such as sphere, cylinder, and ellipsoid, and the one having the smallest parameters and fitting the measured data well was taken. The more realistic structures were then refined to take into account the core, shell, and extent of water penetration, with the overall side and shape being kept similar. Further information about SANS is given in the Supporting Information.

Results and Discussion

Although very short in length, amphiphilic peptide I_3K exhibits a property similar to that of conventional long aliphatic chain surfactants, i.e., a distinct critical aggregation concentration (CAC) in bulk solution. Solubilization of the fluorophore changes its fluorescence peak spectra due to different molecular environments. Such a property has been clearly elucidated by the pyrene fluorescence measurement, in which the ratio of its first and third vibronic bands (I_I/I_{III}) was monitored versus the peptide concentration, as shown in Figure 1. The ratio is very sensitive to the polarity of the environment sensed by pyrene as the probe. Below the CAC, the ratio is high because pyrene senses the polar milieu of water. Above the CAC, the hydrophobic probe is solubilized in the interior of peptide aggregates and senses the nonpolar milieu. The CAC of I_3K was thus determined to be 0.43 mM, corresponding to the intersection point of two straight lines fitting the rapid decreasing region and the low horizontal region.

The formation of well-defined, nanotubular assemblies, with approximate diameters of 10 nm, is evident from the TEM image of I_3K taken at 4 mM (Figure 2a). An impressive feature is that the lengths of these nanotubes mostly exceeded 5 μm when viewed from larger scale images (not shown). Both diameter and length were

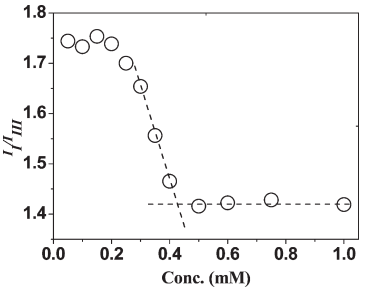

Figure 1. Variation of the pyrene polarity (I_I/I_{III}) with peptide concentration at 25 °C giving an estimate of the CAC of 0.43 mM.

very narrowly distributed. The tubular nature of the peptide assembly is supported by the two parallel lines separated by a dark center region in the TEM images, which is evident from the inset of Figure 2a. Uranyl acetate usually stained the background and left the sample untouched. However, if the sample assemblies were hollow tubular structures, the stain would ingress into their interior, resulting in the dark center within the assembled objects.[6a,14] Note that the occurrence of the inner dark center is completely different from the staining between two contiguous nanotubes as the latter (indicated by red arrows in Figure 2a) is markedly different. As the peptide concentration increased to 10 mM, the peptide nanotubes tended to associate with each other and form branching, as shown in Figure 2b. Very interestingly, the peptide solution at this higher concentration displayed a gel-like feature, which is evident from the rheological measurement (Figure 2c). The storage modulus (G', the elastic component of the complex modulus) was found to be larger than the loss modulus (G'', the viscous component of the complex modulus), with both parameters keeping relatively constant with an oscillatory frequency characteristic of gel materials. It is also interesting to note from panels a and b of Figure 2 that the I_3K nanotubes bear no sign of strong lateral adhesion for the formation of large sheets or bundles. Instead, they show rather strong twisting (as indicated by green arrows in Figure 2b), looking just like twisted cables. Stabilization against clustering or bundling could well arise from the electrostatic repulsion associated with the presence of the positively charged lysine groups on the outer surface of I_3K nanotubes.

Complementary to TEM, AFM enables imaging with excellent lateral and depth resolution. To help resolve the dynamic self-assembly, a 4 mM aqueous solution of I_3K was freshly prepared. After an aliquot of the solution had been deposited on a mica surface for approximately 10 s, the surface was rinsed with pure water and gently dried in a N_2 stream, immediately followed by AFM imaging. AFM phase imaging (Figure 3b) is very effective at revealing the helical structural features compared to topographic height imaging (Figure 3a,c), although both were obtained concurrently from the same scanned surface area. Both left- and right-handed helical ribbons are clearly shown from these images, and there are appreciable

(14) Shao, H.; Parquette, J. R. *Chem. Int. Ed.* **2009**, *48*, 2525.

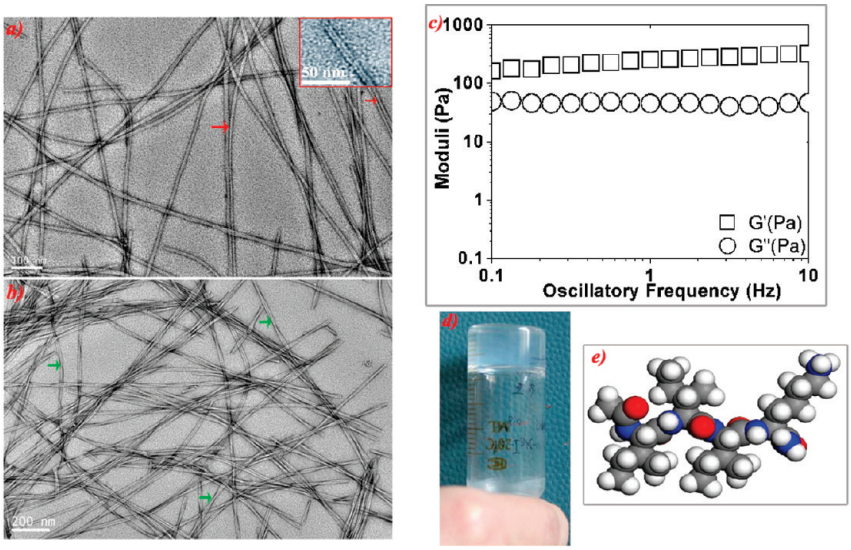

Figure 2. (a) TEM image of I_3K nanotubes in a 4 mM solution at pH 7. The inset is the high-magnification TEM image of a single nanotube showing the dark center between two parallel lines. However, dark central lines indicated by red arrows are indicative of contiguous nanotubes. (b) TEM image of I_3K nanotubes in a 10 mM solution at pH 7, with green arrows showing the twisting. (c) Rheological analysis of the 10 mM I_3K solution at 25 °C. The storage modulus (□), G', and the loss modulus (○), G'', are plotted with respect to oscillatory frequency on log−log scales. (d) Demonstration of the gel setting from the 10 mM I_3K solution by holding it upside down. This sample was aged for more than 3 days. (e) Molecular structure of I_3K. Its fully extended backbone length is ∼1.4 nm, but its fully stretched molecular length is ∼2.0 nm. Color scheme: gray for carbon, white for hydrogen, red for oxygen, and blue for nitrogen.

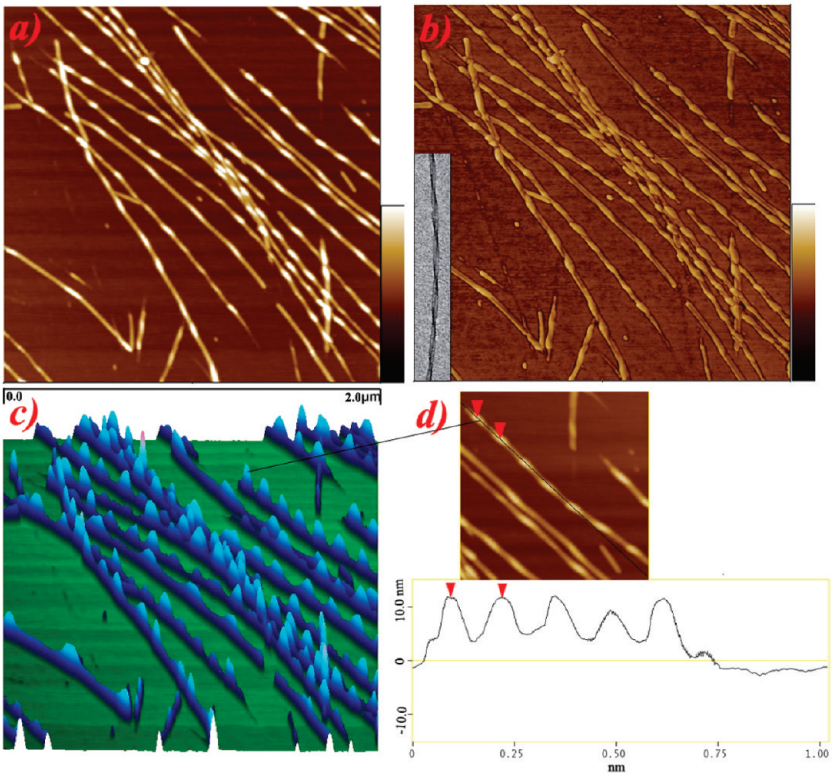

Figure 3. (a) Height AFM image (2 μm × 2 μm) of I_3K helical ribbons, with the Z scale to the right of the image at 20 nm. (b) Corresponding phase image, with the Z scale to the right of the image at 120°. The inset is an exemplar TEM image of a helical intermediate. (c) Corresponding height image presented at a pitch angle of 70° for clear presentation, with the Z scale at 20 nm. (d) Cross-sectional profile along one helical ribbon.

variations in their pitches and pitch angles, suggesting that dynamic peptide self-assembly is likely to proceed from ribbons to tubes with helical ribbons as intermediates. The intermediate structures also exhibit distinguished undulations in height, as evident from the height imaging and profiling (Figure 3d). Note that during the course of our AFM imaging, helical intermediates were dominant and the population of complete tubular structures was low. This was in contrast to the TEM characterization described above where peptide nanotubes with less distinguished helical marking were dominant. Because these images were taken using a freshly prepared solution as compared to the aged solution in TEM imaging, the difference implies that helical ribbons formed at the early stage and were the

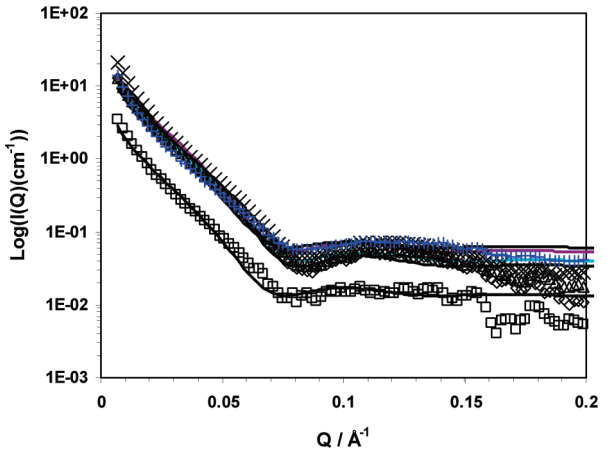

Figure 4. SANS scattering profiles [$I(Q)$] plotted vs neutron wave vector (Q) for I_3K at 10 mM and pH 5 (◇), 7 (△), 9 (×), and 7 with 0.1 M NaCl (+), as well as that (□) of 3 mM I_3K at pH 7. The fittings for I_3K revealed the formation of nanocylinders with diameters of 10 nm and lengths of > 100 nm. Changes in pH and addition of 0.1 M NaCl did not cause any major changes away from this cylindrical shape. The measurement at 3 mM I_3K fitted to the same nanocylindrical shape well, and the difference could be entirely ascribed to the peptide concentration.

intermediates toward the final nanotubes. In fact, when the freshly prepared solution was used for TEM characterization, helical intermediates were also observed (e.g., see the inset of Figure 3b). Because of the convolution between the AFM tip and the sample, the lateral dimension of the scanned object is usually broadened but the vertical one is little influenced. As shown in Figure 3d, the height profile revealed that the peak of the helical intermediates is some 12 nm in height. This value is slightly larger than the diameters of the fully grown peptide nanotubes, suggesting a slight narrowing during the structural transition.

Helical structures have been observed for a number of systems, including amphiphiles, bile salts, diblock polymers, and β-sheet peptides. In these systems, the helical structures have been widely regarded as precursors in the growth of tubules or fibrils.[15−20] The underlying mechanisms have been extensively discussed by Schnur et al.,[15] Benedek et al.,[16] and Boden et al.[18] These authors have attributed the formation of helical structures to molecular chirality, which not only limits the lateral growth of ribbons or tapes but also favors their twisting. I_3K is composed of L-amino acid residues and has an intrinsic propensity to adopt the β-sheet structure. It prefers to form ribbons or other twisting intermediates leading to the fully developed nanotubes.

The solutions of I_3K at different pH values were studied by small angle neutron scattering (SANS) with the measured scattering intensity profiles shown in Figure 4. The SANS profiles for I_3K at a peptide concentration of 10 mM were very similar in shape and level, and the difference was very small, showing very similar nanostructures formed at different pH values and ionic strengths. Data analysis for the measured scattering profiles revealed the formation of nanocylinders with diameters of ~10 nm and lengths of > 100 nm, consistent with the AFM and TEM observations. In contrast, models of spheres and short ellipsoids were inappropriate for generating the right shape of scattering profiles. Dilution to an I_3K concentration of 3 mM did lower the level of the scattering profile, but the shape was identical to those at high concentrations. Indeed, the profile was fitted with the identical nanocylinders, and the difference was completely ascribed to the concentration difference.

The analysis described above has not taken into account the inner cavities within the nanotubes to keep the number of variables at the minimal level. As indicated previously from TEM, the I_3K nanotubes have inner cavities. The subsequent analysis was conducted using the core−shell cylinder model, and the optimal fitting led to an outer diameter of 10−11 nm, an inner diameter of 5−6 nm, a shell thickness of 2.5−3.0 nm, and a length of > 1000 nm. The lack of sensitivity in this case might arise from the very small inner diameter coupled with the extreme long nanotube length.

In comparison, the SANS scattering profiles from L_3K (Figure S3 of the Supporting Information) were very different from those of I_3K, showing a completely different nanostructure. On the other hand, as in the case of I_3K, all L_3K profiles were similar to themselves, suggesting that changes in solution concentration and pH did not affect the main structural feature. Data analysis for these profiles revealed the formation of nanospheres with diameters of ~10−15 nm. While these values are broadly consistent with those observed via TFM (as will be shown later), the strong polydispersity and the lack of knowledge about size distribution constrained further analysis about the structure inside nanospheres.

Circular dichroism (CD) and Fourier transform infrared spectroscopy (FTIR) were employed to assess the molecular configurations within the assembled nanostructures of I_3K. The CD spectrum (Figure 5a) measured from the 10 mM I_3K solution displayed a positive peak at 195 nm and a negative peak at 220 nm, characteristic of the formation of β-sheet structure. This result was supported by the FTIR analysis with the same peptide solution under the attenuated total reflection (ATR) mode with the solvent contribution to the overall spectrum subtracted from the sample spectrum of interest. The amide I band, which arises predominantly from the stretching vibration of the peptide carbonyl groups and occurs in the region of 1600−1700 cm^{-1}, is sensitive to changes in the secondary structures and has been most

(15) (a) Schnur, J. M. *Science* **1993**, *262*, 1669. (b) Georger, J. H.; Singh, A.; Price, R. R.; Schnur, J. M.; Yager, P.; Schoen, P. E. *J. Am. Chem. Soc.* **1987**, *109*, 6169. (c) Selinger, J. V.; Spector, M. S.; Schnur, J. M. *J. Phys. Chem. B* **2001**, *105*, 7157.
(16) (a) Chung, D. S.; Benedek, G. B.; Konikoff, F. M.; Donovan, J. M. *Proc. Natl. Acad. Sci. U.S.A.* **1993**, *90*, 11341. (b) Zastavker, Y. V.; Asherie, N.; Lomakin, A.; Pande, J.; Donovan, J. M.; Schnur, J. M.; Benedek, G. B. *Proc. Natl. Acad. Sci. U.S.A.* **1999**, *96*, 7883.
(17) Cornelissen, J.; Fischer, M.; Sommerdijk, N.; Nolte, R. J. M. *Science* **1998**, *280*, 1427.
(18) (a) Nyrkova, I. A.; Semenov, A. N.; Aggeli, A.; Boden, N. *Eur. Phys. J. B* **2000**, *17*, 481. (b) Aggeli, A.; Nyrkova, I. A.; Bell, M.; Harding, R.; Carrick, L.; Mcleish, T. C. B.; Semenov, A. N.; Boden, N. *Proc. Natl. Acad. Sci. U.S.A.* **2001**, *98*, 11857.
(19) Marini, D. M.; Hwang, W.; Lauffenburger, D. A.; Zhang, S.; Kamm, R. D. *Nano Lett.* **2002**, *2*, 295.
(20) Lu, K.; Jacob, J.; Thiyagarajan, P.; Conticello, V. P.; Lynn, D. G. *J. Am. Chem. Soc.* **2003**, *125*, 6391.

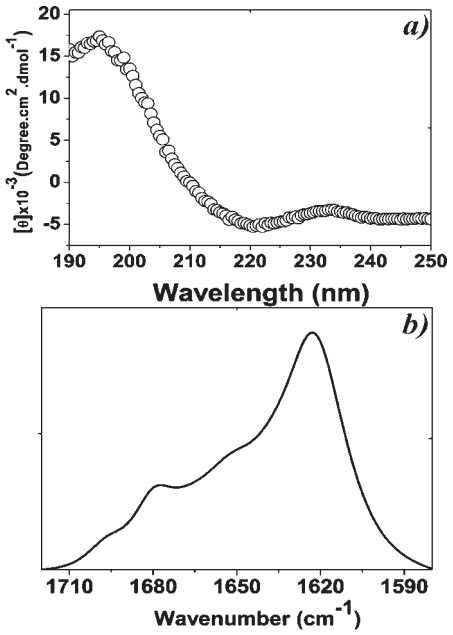

Figure 5. (a) CD and (b) FTIR spectra (amide I region) of the I_3K solution measured at pH 7 and 22−23 °C. These spectra revealed β-sheet structure formation, and an increase in concentration form 4 to 10 mM caused little variation in the secondary structure, though the solution viscosity did increase substantially.

widely used to assess the structural conformations of peptides. Each type of secondary structures tends to give rise to a different C−O stretching frequency in the amide I region of the spectrum.[21] Figure 5b shows an intense amide I band at 1622 cm^{-1} and a weak band at 1678 cm^{-1}. The band at 1622 cm^{-1} is relatively strong and is characteristic of a high content of β-sheet structure. The weak band at the high wavenumber of 1678 cm^{-1} is possibly associated with an antiparallel β-sheet conformation.[21b,22] More detailed structural analyses such as solid-state NMR, as suggested by Lynn et al.,[23] will be necessary to further associate the main structural features at different structural levels.

On the basis of the results presented above, we can outline the dynamic self-assembly process of I_3K using the simple model schematically shown in Figure 6. First, I_3K molecules associate into small peptide fragments (Figure 6A) that are composed of interdigitated bilayers with their charged C-terminal lysine residues projected on both sides of the surface and the hydrophobic isoleucine residues kept in the interior. Second, small peptide fragments then assemble into ribbons, with growth mainly occurring along the hydrogen bonding direction within these antiparallel β-sheets (Figure 6B). Note that the lateral growth is driven by the hydrophobic affinity between isoleucine side chains and is balanced by hydrogen

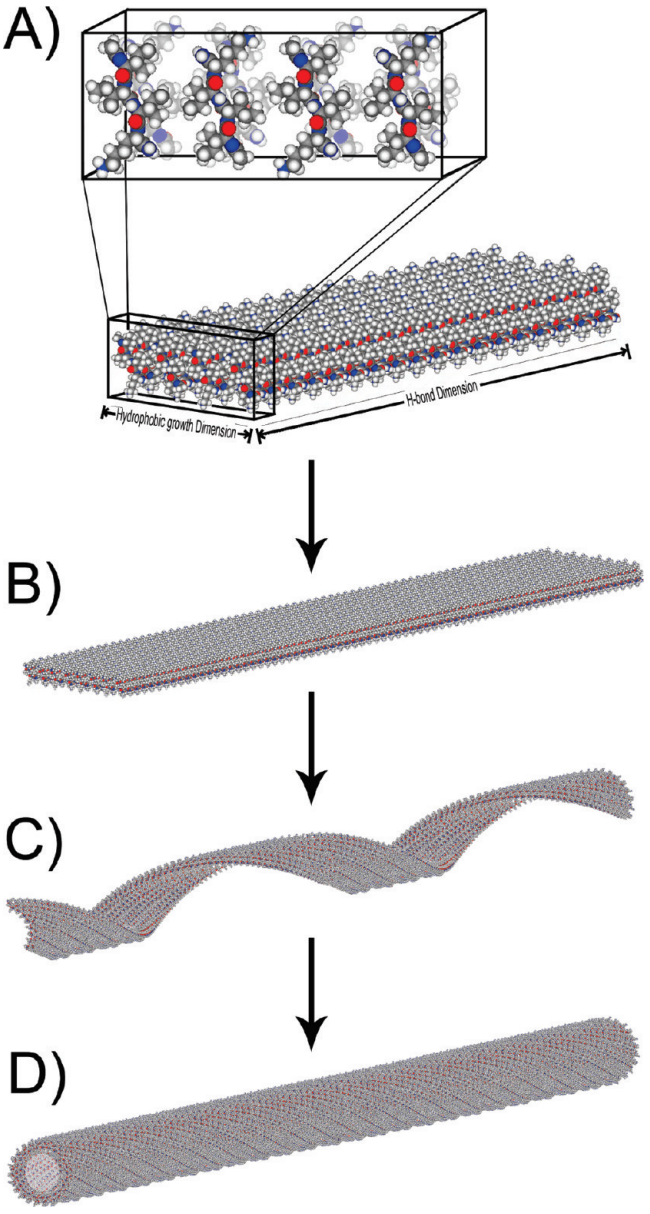

Figure 6. Schematic representation of the I_3K self-assembly process leading to the formation of peptide nanotubes.

bonding, and the surface curving and twisting inherent to the chirality and the electrostatic repulsion between surface lysine residues. Third, as ribbons grow they tend to twist because of molecular chirality and surface curving (Figure 6C). Finally, as the helical ribbons further grow, the twisting force becomes more intensified along the main axis and drives the edges of the helical ribbons to fuse, resulting in the formation of nanotubes (Figure 6D).

Thus, hydrophobic interaction and hydrogen bonding were dominant in the initial stage of the formation of twisted I_3K β-sheet fragments. With the ribbon growing, longer-range interactions then became dominant. The characteristic β-sheet promoting feature of isoleucine played a key role in the structural packing and surface twisting. When isoleucines were replaced with leucines, the resulting L_3K (its CAC was ~1.1 mM) formed nanospheres. TEM imaging revealed that the diameters were in the range of 8−25 nm under the same solution conditions

(21) (a) Dong, A.; Huang, P.; Caughey, W. S. *Biochemistry* **1990**, *29*, 3303. (b) Haris, P. I.; Chapman, D. C. *Biopolymers* **1995**, *37*, 251.
(22) (a) Krysmann, M. J.; Castelletto, V.; Kelarakis, A.; Hamley, I. W.; Hule, R. A.; Pochan, D. J. *Biochemistry* **2008**, *47*, 4597. (b) Pelton, J. T.; McLean, L. R. *Anal. Biochem.* **2000**, *277*, 167. (c) Collier, J. H.; Hu, B.-H.; Ruberti, J. W.; Zhang, J.; Shum, P.; Thompson, D. H. *J. Am. Chem. Soc.* **2001**, *123*, 9463.
(23) Benzinger, T. L. S.; Gregory, D. M.; Burkoth, T. S.; Miller-Auer, H.; Lynn, D. G.; Botto, R. E.; Meredith, S. C. *Proc. Natl. Acad. Sci. U.S.A.* **1998**, *95*, 13407.

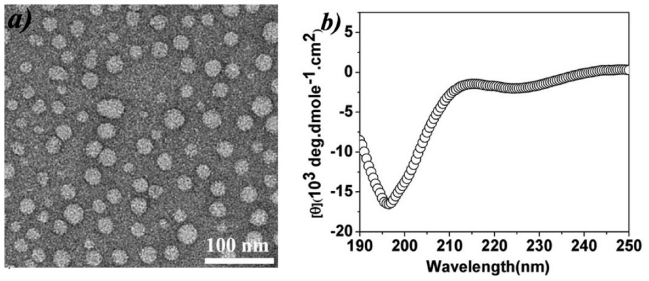

Figure 7. (a) TEM image of L_3K (Ac-L_3K) indicating the formation of spherical aggregates with a diameter of 8−25 nm under the same solution conditions that were studied for I_3K. (b) Corresponding CD analysis, indicating the combination of most random coil and minor α-helix structures associated with the L_3K nanoassemblies.

that were used for I_3K, and the sizes as presented in Figure 7 appear to be dominated by some large ones, in comparison with those determined from SANS measurements (Figure S3 of the Supporting Information). SANS offered in situ probing of the sizes, and the difference indicated possible deformations during the TEM sample preparation. The corresponding CD analysis indicated the combination of most random coil and minor α-helix structures associated with the L_3K nanoassemblies (Figure 7b). Such a marked difference in the assembled nanostructures could be associated with the different structural characters of leucine and isoleucine. Leucine usually shows a strong propensity to form α-helix structure, while isoleucine favors the β-sheet conformation.[13] As suggested by Paramonov et al.,[24] β-sheet hydrogen bonding is essential for main axial growth. Thus, the contribution of hydrogen bonding in the case of L_3K must be weak if ever present, and instead, hydrophobic interaction must be the dominant driving force for the self-assembly leading to the formation of spherical aggregates.

I_3K nanotubes exhibited an exceptional stability against heating and washing by organic solvents. After the mature nanotubes had been incubated in a water bath at 60 °C for 0.5 h, no variations in their morphologies were detected in either the tubular feature or the secondary structure (Figure S4 of the Supporting Information). We assessed the stability of I_3K nanotubes in organic solvents by mixing the mature peptide nanotubes with different solvents, including methanol, ethanol, acetone, and acetonitrile, and then incubating the solutions at ambient temperature for at least 24 h. The corresponding TEM and CD measurements did not indicate any major variations in the morphology and secondary structure of the tubular assemblies either (data not shown). The high stability of the I_3K nanotubes again worked as testimony to the strength of hydrophobic interaction combined with hydrogen bonding within the peptide nanotubes.

The high stability and robustness of I_3K nanotubes are attractive for their use as templates for nanotechnology applications. Lysine contains a primary amine and is particularly abundant in silaffins (silica-precipitating proteins found in diatoms). It has long been perceived to facilitate biosilicification in nature, and consequently, synthetic molecules containing this amino acid residue have been applied for biomimetic silicification under mild conditions.[4b,25,26] In these investigations, lysine is thought to be responsible for not only catalyzing the hydrolysis of organosilicate precursors such as TEOS (tetraethoxysilane) and TMOS (tetramethoxysilane) but also promoting the aggregation and condensation of weak negative silicate species, eventually producing silica precipitates. As a result, if I_3K nanotubes are employed for silica synthesis, the formation of silica nanotubes would be expected to occur, provided that the lysine residues could promote silica deposition. While many factors might affect the growth of the silica layers deposited on the inner and outer surfaces, the surface charge density of lysine groups is thought to be important in regulating and controlling silica layer thicknesses via charge neutralization under the reaction conditions.

In the hydrolysis study, TEOS was used as a silica precursor. In a typical preparation, 40 μL of TEOS was dissolved in 2 mL of ethanol, followed by their mixing with the equal volume of an I_3K aqueous solution (4 mM) at pH 7. After incubation at ambient temperature for 1 week, a transparent gel-like precipitate was obtained following the centrifugation of the sample for 30 min at 30000 rpm. The silica/peptide precipitate collected was lyophilized, and the resulting powder was copiously rinsed with ethanol and water. After lyophilization again, the powder was calcinated at 550 °C for 8 h to remove the peptide template and was subsequently characterized by TEM without staining. As shown in Figure 8, TEM analysis revealed the formation of hollow silica nanotubes templated by the I_3K nanotubes. Compared with the silica-coated peptide nanotubes that were well separated and were clearly visible even without staining (Figure S5 of the Supporting Information and inset of Figure 8a), silica nanotubes became highly aggregated, possibly because of adhesion after calcination. In addition, the control experiment in the absence of I_3K was also performed under the same conditions. No precipitate was collected after incubation and centrifugation as expected, indicating no occurrence of silicification.

There are some erected silica nanotubes as indicated by the red arrows in Figure 8b, and their walls are distinguishingly clear because of high electron density. As a result, the geometrical dimensions of these silica nanotubes are easily determined: the inner diameter is ca. 5.5 nm, and the outer diameter is ca. 13 nm. The wall is thus rather thick (~3.7 nm). Furthermore, selective electron area diffraction (SEAD) indicated the amorphous nature of the deposited silica, as shown in the inset of Figure 8b.

(24) Paramonov, S. E.; Jun, H.-W.; Hartgerink, J. D. *J. Am. Chem. Soc.* **2006**, *128*, 7291.

(25) (a) Dickerson, M. B.; Sandhage, K. H.; Naik, R. R. *Chem. Rev.* **2008**, *108*, 4935. (b) Jan, J. S.; Lee, S.; Carr, C. S.; Shantz, D. F. *Chem. Mater.* **2005**, *17*, 4310. (c) Yuwono, V. M.; Hartgerink, J. D. *Langmuir* **2007**, *23*, 5033. (d) Patwardhan, S. V.; Mukherhee, N.; Steinitz-Kannan, M.; Clarson, S. J. *Chem. Commun.* **2003**, 1122.

(26) Pouget, E.; Dujardin, E.; Cavalier, A.; Moreac, A.; Valéry, C.; Marchi-Artzner, V.; Weiss, T.; Renault, A.; Paternostre, M.; Artzner, F. *Nat. Mater.* **2007**, *6*, 434.

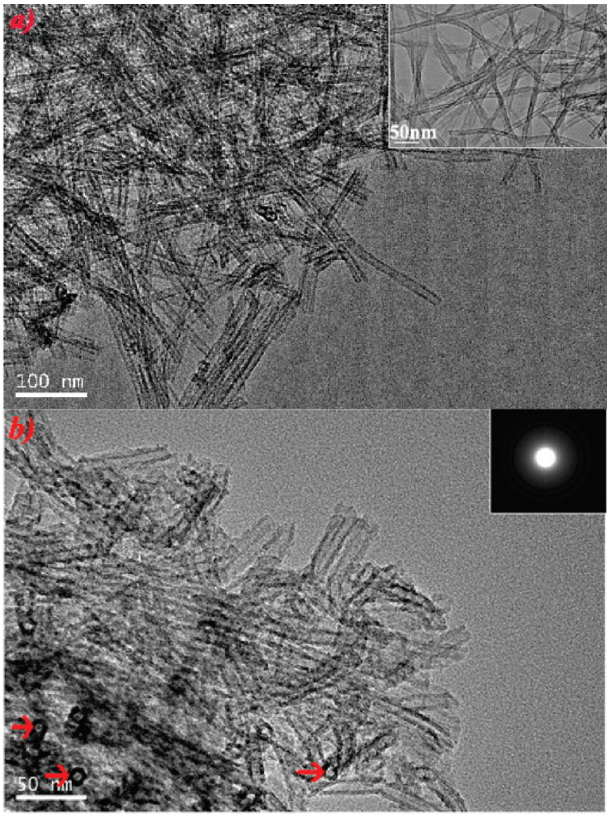

Figure 8. TEM images of I_3K-templated silica nanotubes after calcinations: (a) main feature of clustering of silica nanotubes after calcination in contrast to the well-separated nanotubes shown in the inset before calcinations and (b) uniform appearance of silica nanotubes and their walls, and the presence of some nanotubes with open ends allowing the diameters and wall thickness to be measured. The SEAD pattern in the inset of Figure 8b indicates the amorphous nature of the resulting silica.

Fabrication of inorganic nanomaterials with well-defined shape and size has been extensively pursued by chemists and material scientists. Silica nanotubes are of particular interest to catalysis, separation, sensing, and drug delivery.[27] Typical synthetic chemistry of silica suffers from harsh preparative conditions, such as extreme pH, high temperature, and high pressure. In contrast, living organisms such as diatoms, sponges, and higher plants are capable of producing a variety of biogenic silica with complex structures at neutral pH at ambient temperature and pressure. Studies of biosilicification have revealed the functional involvement of some biomacromolecules in the formation of biogenic silica, including silaffins, silicateins, and long chain polyamines, and highlighted their roles in controlling silica formation.[28,29] Inspired by these biological processes, we have used the short amphiphilic peptide I_3K containing lysine residues to mimic the performance of the biomolecules mentioned above. Our results show that this peptide readily self-assembled into nanotubes in aqueous solution at neutral pH. Because these peptide nantubes have relatively high stability and the lysine residues are distributed on the surfaces of the nanotubes, they worked successfully as templates to induce the formation of silica nanotubes under mild physiological conditions. Unlike other cationic alkyl surfactants that have been used to template the formation of silica, this amphiphile is entirely composed of amino acid residues. Moreover, a few natural or designed peptide sequences such as R5[30] and P11-3[4b] have been used to mediate silica formation, but these peptides generally consisted of 10 or more amino acids. To the best of our knowledge, I_3K is the shortest peptide that is used to control silicification, leading to the formation of silica nanotubes. Because it is easy to synthesize the short chain templating molecules such as I_3K, we believe this work is particularly relevant to the biomimetic fabrication of silica nanotubes on a large scale.

Conclusions

L_3K and I_3K are among the shortest de novo designed amphiphilic peptides, but they are extremely effective at forming stable nanostructures in aqueous solution. Our studies show that while L_3K self-assembled into nanospheres I_3K formed long nanotubes. The morphological differences were attributed to the structural difference between leucine and isoleucine. The CD and IR studies revealed the different secondary structures formed in the respective nanostructures, suggesting the dominant role of hydrophobic interaction in the formation of L_3K nanospheres and of the hydrogen bonding associated with the templating of antiparallel β-sheet I_3K fragments and the eventual formation of the twisted I_3K nanotubes.

The highly stable I_3K nanotubes were used as templates for fabricating silica nanotubes. After the introduction of TEOS, the silicification reaction occurred on the inner and outer peptide nanotube surfaces and the process was catalyzed by surface-exposed lysine residues, resulting in the formation of silica nanotubes. Because peptide self-assembly forms stable nanotemplates under mild aqueous conditions, the route demonstrated in this work is attractive for the practical production of nanostructured inorganic materials under benign conditions. Furthermore, because the size, shape, and twisting of the nanotemplates could be

(27) (a) Kresge, C. T.; Leonowicz, M. E.; Roth, W. J.; Vartuli, J. C.; Beck, J. S. *Science* **1992**, *359*, 710. (b) Minakuchi, H.; Nakanishi, K.; Soga, N.; Ishizuka, N.; Tanaka, N. *Anal. Chem.* **1996**, *68*, 3498. (c) Slowing, I. I.; Trewyn, B. G.; Giri, S.; Lin, V. S. Y. *Adv. Funct. Mater.* **2007**, *17*, 1225. (d) Chen, J.-F.; Ding, H.-M.; Wang, J.-X.; Shao, L. *Biomaterials* **2004**, *25*, 723–727. (e) Barbé, C.; Bartlett, J.; Kong, L.; Finnie, K.; Lin, H. Q.; Larkin, M.; Calleja, S.; Bush, A.; Calleja, G. *Adv. Mater.* **2004**, *16*, 1959.

(28) (a) Kröger, N.; Deutzmann, R.; Sumper, M. *Science* **1999**, *286*, 1129. (b) Kröger, N.; Deutzmann, R.; Bergsdorf, C.; Sumper, M. *Proc. Natl. Acad. Sci. U.S.A.* **2000**, *97*, 14133. (c) Kröger, N.; Lorenz, S.; Brunner, E.; Sumper, M. *Science* **2002**, *298*, 584. (d) Poulsen, N.; Sumper, M.; Kröger, N. *Proc. Natl. Acad. Sci. U.S.A.* **2003**, *100*, 12075. (e) Poulsen, N.; Kröger, N. *J. Biol. Chem.* **2004**, *278*, 42993. (f) Sumper, M.; Kröger, N. *J. Mater. Chem.* **2004**, *14*, 2059.

(29) (a) Shimizu, K.; Cha, J.; Stucky, G. D.; Morse, D. E. *Proc. Natl. Acad. Sci. U.S.A.* **1998**, *95*, 6234. (b) Cha, J. N.; Shimizu, K.; Zhou, Y.; Christiansen, S. C.; Chmelka, B. F.; Stucky, G. D.; Morse, D. E. *Proc. Natl. Acad. Sci. U.S.A.* **1999**, *96*, 361. (c) Zhou, Y.; Shimizu, K.; Cha, J. N.; Stucky, G. D.; Morse, D. E. *Angew. Chem., Int. Ed.* **1999**, *38*, 779.

(30) Naik, R. R.; Whitlock, P. W.; Rodriguez, F.; Brott, L. L.; Glawe, D. D.; Clarson, S. J.; Stone, M. O. *Chem. Commun.* **2003**, 238.

(31) King, S. M. In *Modern Techniques for Polymer Characterisation*; Pethrick, R. A., Dawkins, J. V., Eds.; Wiley: New York, 1999; Chapter 7.

easily controlled by altering the molecular structure of peptides, the use of ultrashort peptides could well become advantageous over many other existing approaches.

Acknowledgment. This work was supported by the National Natural Science Foundation of China (Grant 20773164) and the Royal Society (London) under a Sino-British Fellowship Trust grant.

Supporting Information Available: Peptide synthesis and purification, SANS theory, and Figures S1−S5. This material is available free of charge via the Internet at http://pubs.acs.org.